Characterization of piezoelectric micromachined ultrasonic transducers for biomedical applications

Bruno Fain, Francois Blard, Jean-Rémi Chatroux, Romain Liechti, Fabrice Casset, Antoine Hamelin, Jean Claude Bastien, Hélène Lhermet

▶ **To cite this version:**

Bruno Fain, Francois Blard, Jean-Rémi Chatroux, Romain Liechti, Fabrice Casset, et al.. Characterization of piezoelectric micromachined ultrasonic transducers for biomedical applications. 2023 22nd International Conference on Solid-State Sensors, Actuators and Microsystems (Transducers), Jun 2023, Kyoto, Japan. pp.116-119. cea-04665736

HAL Id: cea-04665736
https://cea.hal.science/cea-04665736

Submitted on 31 Jul 2024

HAL is a multi-disciplinary open access archive for the deposit and dissemination of scientific research documents, whether they are published or not. The documents may come from teaching and research institutions in France or abroad, or from public or private research centers.

L'archive ouverte pluridisciplinaire **HAL**, est destinée au dépôt et à la diffusion de documents scientifiques de niveau recherche, publiés ou non, émanant des établissements d'enseignement et de recherche français ou étrangers, des laboratoires publics ou privés.

CHARACTERIZATION OF PIEZOELECTRIC MICROMACHINED ULTRASONIC TRANSDUCERS FOR BIOMEDICAL APPLICATIONS

Bruno Fain, François Blard, Jean-Rémi Chatroux, Romain Liechti, Fabrice Casset, Antoine Hamelin, Jean-Claude Bastien and Hélène Lhermet*
CEA Leti, Univ. Grenoble Alpes, F-38000 Grenoble, France

ABSTRACT

We report a study of AlN-based piezoelectric micromachined ultrasonic transducers (PMUT) dedicated to biomedical applications. The fabrication, the packaging, the electrical and acoustical characterization of the devices are reported and compared with the expectations. The device exhibits a 35% -3dB bandwidth with a central frequency at 10.4 MHz. The drive sensitivity is measured at 0.63 kPa/V/mm² and the receive sensitivity at 570 µA/MPa/mm². This confirms the potential of PMUT as low-voltage, miniaturized ultrasound transducers for biomedical applications.

KEYWORDS

Piezoelectric micromachined ultrasound transducers (PMUT), array, acoustics

INTRODUCTION

During the last decades, the PMUT technology has gained more and more interest as a promising field of research that could address some challenges in various domains such as fingerprint sensing [1], range finding [2], gesture recognition [3] and biomedical applications [4]–[7]. As a microelectromechanical system technology, PMUT can provide some keys to overcome the current limitations of standard piezoceramic transducers and open new applications fields thanks to miniaturization, cMOS co-integration and batch fabrication cost. For biomedical applications, capacitive and piezoelectric micromachined ultrasonic transducers are promising to build 2D arrays and for miniaturization purpose. Furthermore, PMUT require relatively lower DC voltages than their capacitive counterparts, what may ease the associated electronics.

Biomedical applications encompass a variety of ultrasonic modalities. Each application, such as focused ultrasound for ablation, gynaecology or intravascular ultrasound, presents its own set of specifications. As reported in [8], there is still no clear consensus of which technology is better suited for each biomedical or clinical needs. The PMUT field is still evolving, regarding both PMUT design and piezoelectric material. During the recent years, advanced PMUT with ring-shaped [6], annular-shaped [9] or island-shaped [10] geometry have been proposed to reach higher performance. Materials such as epitaxial PZT [7] or KNN [11] are being considered as an alternative to poly-crystalline PZT.

In this paper, we report a study of AlN-based PMUT, that present good characteristic for sensing due to the intrinsic properties of AlN. Moreover, AlN-based PMUT are promising as lead-free devices and may be co-integrated with CMOS technology. This study covers the design, the fabrication, the electromechanical and acoustical characterization of an AlN-based PMUT.

DESIGN AND FABRICATION

The PMUT geometry is presented in Figure 1. The array configuration consists of 96 cells with a 200-µm pitch. Each cell is 190-µm wide, 5-mm high, and encompasses three columns of 76 circular membranes. The diameter of each single membrane is defined by the underlying cavity at 53 µm. Supplementary devices exhibiting 45 µm, 49 µm and 57 µm-wide membranes have also been designed for comparison purposes.

The membrane stack consists in a 100-nm thick SiO_2 layer, a 1500-nm thick elastic Si layer, the piezoelectric stack Mo (200 nm) / AlN (900 nm) / AlCu (200 nm), and a 300 nm-thick SiN passivation layer. Metallic TiNiAu is used to form the bonding pads.

At the single cavity stage, the bottom electrode covers the whole cavity and the top electrode is patterned to form a circle with a diameter of 31.5 µm corresponding to 60 % of the cavity diameter, what optimizes the sensitivity of the PMUT. The electrodes of a cell are connected together so that the cell may be driven or sensed using only two electrical connections. Both the bottom and top electrodes are patterned to reduce parasitic capacitance. The bottom electrode of the different cells are all connected together to the ground. The pads are located 500 µm away from the active area to ease the packaging process.

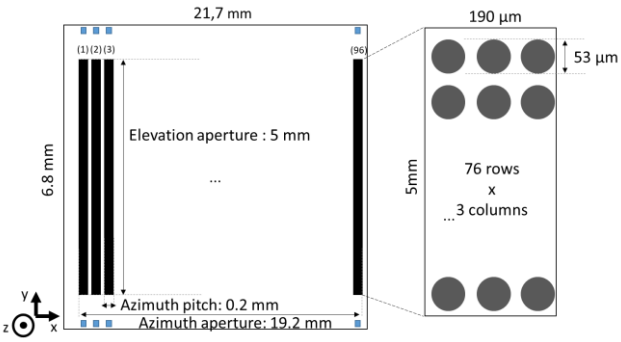

Figure 1: Layout of the PMUT device. The die is composed of 96 cells, each of them is made of 76 X 3 53µm – wide circular diaphragms. The pads (in blue) are positioned away from the diaphragms to ease the wire-bonding and packaging process.

The process flow is presented in Figure 2. It is based on the fabrication of a cavity SOI as in [12], using a 8'' MEMS platform with a precise control of lateral dimensions. First, 10 µm-deep cavities are etched within a first Si wafer (a). Second, a SOI wafer is covered with a 100 µm-thick

SiO_2 (b) layer and bonded to the first Si wafer using direct wafer bonding technologies (c). The handle and the buried oxide layer are removed to keep the Si layer and the SiO_2 layer on top of the cavity (d). At this stage, a particular attention is paid to obtain a low roughness, which is mandatory to obtain good AlN properties. Then, the bottom Mo layer is deposited and etched, followed by the deposition of the AlN layer and the top AlCu electrode (e). The top electrode is patterned, then the AlN layer is etooched at the pads location. The SiN passivation layer is deposited and opened at the pads location. Finally, the TiNiAu contact pads are achieved (f).

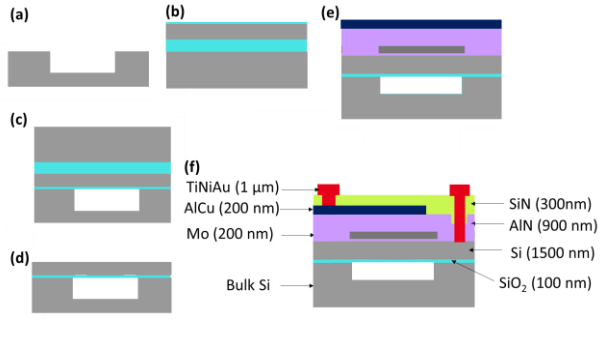

Figure 2: Schematic of the process flow. (a) Si wafer patterned and etched to form cavities (b) SOI wafer with additional top SiO_2 layer (c) Direct wafer bonding of the two wafers in vacuum (d) Removal of the handle and the buried oxide layer (e) Deposition of the piezoelectric stack Mo/AlN/AlCu (f) Final device after passivation and contacts

After wafer-level characterization, single dies are connected to a dedicated PCB by standard wire bonding. The bondings are covered with an encapsulation resin then the whole PCB is covered with parylene for acoustic characterization in water (Figure 3).

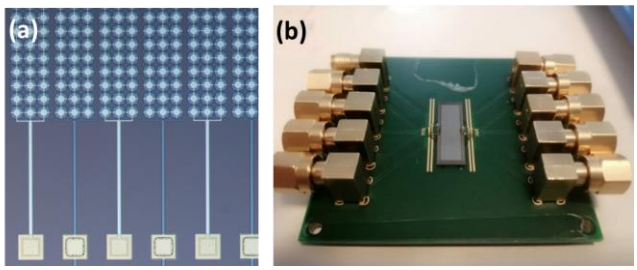

Figure 3: Optical picture of a PMUT device (a) and of a device reported on the dedicated PCB card (b).

SIMULATION

The simulation step includes the design of the single membrane, the calculation of the self-radiation impedance, the calculation of the mutual radiation impedance with the other membranes of the cell, the directivity, the absorption and the propagation to compute the total acoustic pressure. Here, we detail the simulation of a single membrane.

The design of the single membrane has been defined using finite element modelling and analytical means based on the lumped element formulation presented in [13]. An

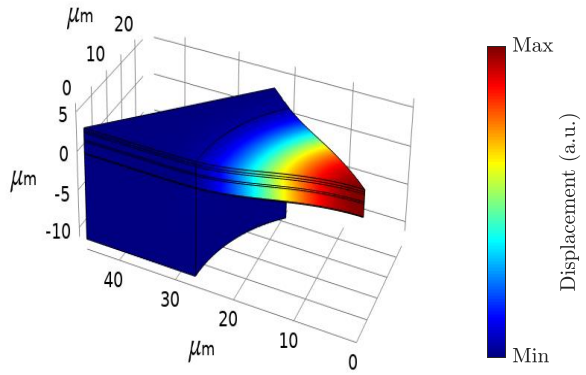

Figure 4: Displacement amplitude normalized to the maximum for an eighth of a single circular PMUT transducer (Comsol multiphysics)

eighth of a membrane has been simulated using Comsol Multiphysics, as we are only interested by the frequency band around the first mode of the structure (Figure 4). As a first step, the resonance frequency of a single membrane without parylene has been simulated with an eigenfrequency study, assuming that natural and resonance frequencies are close to each other since the quality factor is high (>100). A portion of the periphery of the membrane is included in the finite element model to simulate an imperfect clamp. In the analytical model, an equivalent anchorage stiffness is formulated as a series equivalent stiffness whose value is dependent on the inverse of the square of the radius. Figure 5 presents the resonance frequency as a function of the radius of the membrane. Both models are reasonably close for a radius ranging from 15 to 40 µm. Below 15 µm, the thin plate assumption is incorrect, and it results in an over estimation of the resonance frequency by the analytical model compared to the finite element model. For a radius larger than 40 µm, another study has shown that the residual stress, not taken into account into the analytical model, is significantly affecting the resonance frequency. The results do correspond to the experimental resonance frequency deduced from electromechanical measurements presented in next section.

The analytical model is then completed to describe the behavior of the whole cell, in air and in water, what is beyond the scope of this paper.

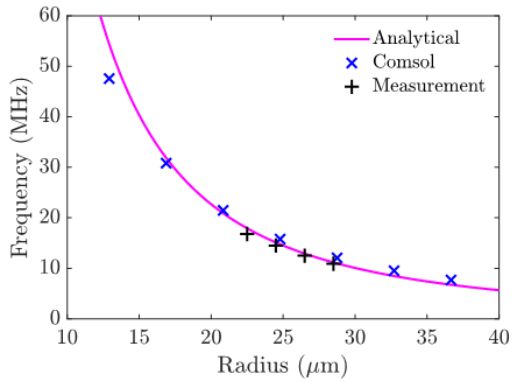

Figure 5: Resonance frequency of a single membrane in air without parylene estimated with the analytical and the finite element models. Experimental values deduced from electromechanical measurements are plotted in black.

ELECTROMECHANICAL CHARACTERIZATION

The in-air electrical characteristics of the PMUT device have been measured through impedance analysis. A measurement of one cell is presented in Figure 6, revealing a capacitance of 28.1 pF by a fit with a Butterworth-Van Dyke analytical model. Optical characterization of a single membrane is also achieved (Figure 7) using laser Doppler vibrometry and fitted with a second-order harmonic oscillator model. Note that the impedance measurements reflect the collective behavior of the 228 membranes of a cell, whereas the optical measurement corresponds to a single membrane. This explains why the quality factor derived from impedance measurement, that reflects both the single membrane properties and the small discrepancies between the membranes of the cell, is lower (70) than that directly deduced from optical measurement (250). Nevertheless, the resonance frequencies are consistent because the mutual radiation impedance does not play an important role when surrounding medium is air. The resonance frequency in air is typically measured at 12.8 MHz without parylene, which is in good agreement with the simulations, as shown in Figure 5. The die-to-die variation is about 100 kHz and is due to residual stress variations within the AlN layer [14].

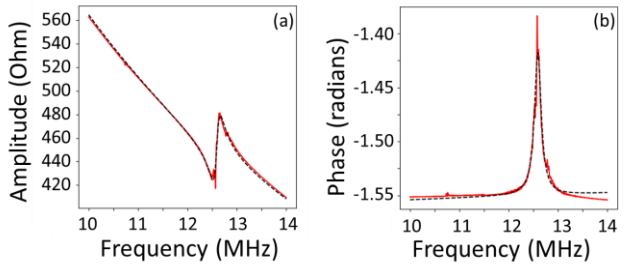

Figure 6: Impedance measurement of one cell in air: (a) amplitude and (b) phase. Red lines: experiments. Dashed black lines: analytical model.

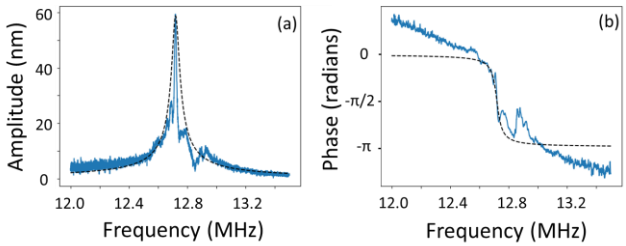

Figure 7: Optical measurement of the displacement of a single membrane in the air: (a) amplitude and (b) phase. The actuation voltage is 1V. Blue lines: experiments. Dashed black lines: analytical model.

ACOUSTICAL CHARACTERIZATION

The PMUT is characterized in water, first as an emitter. The emitted acoustic pressure of a single cell is measured with a calibrated hydrophone, as a function of the distance (Figure 8). A 10-periods-long actuation signal is used to actuate the PMUT at a frequency of 10 MHz. Typical output pressure is 0.23 kPa/V_{pp} at 10 cm, which may be converted into a surface pressure per area of 0.63 kPa/V_{pp}/mm² and an absorption coefficient of 0.86 dB/cm^{-1} using a fit of the data.

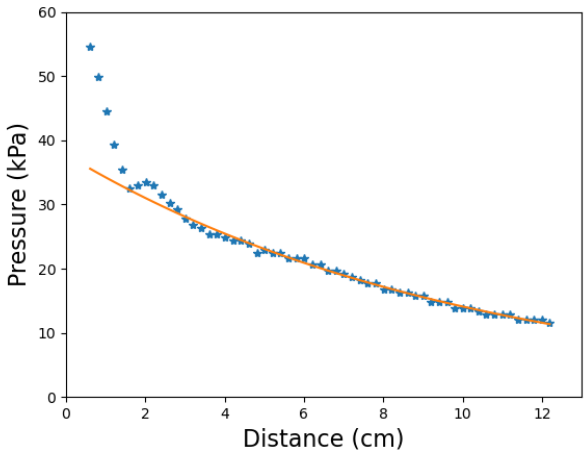

Figure 8: Output pressure as a function of distance for a single cell, for a peak-to-peak actuation voltage of 60V. Blue: experimental measurements. Orange: Fit of the far field measurement with $P = P_0 . 10^{-\frac{\alpha d}{20}} V_{pp}$*, where* P_0 *is the surface pressure per volt, d is the distance and* V_{pp} *is the peak-to-peak actuation voltage.*

The frequency-dependent output pressure is measured using a 50 ns-long pulse signal. The output pressure at 10 cm, normalized by the sensitivity of the hydrophone and the spectrum of the actuation signal, is presented in Figure 9. The central frequency of the device in water is 10.4 MHz with a 35% bandwidth. This result is in good agreement with the analytical simulation.

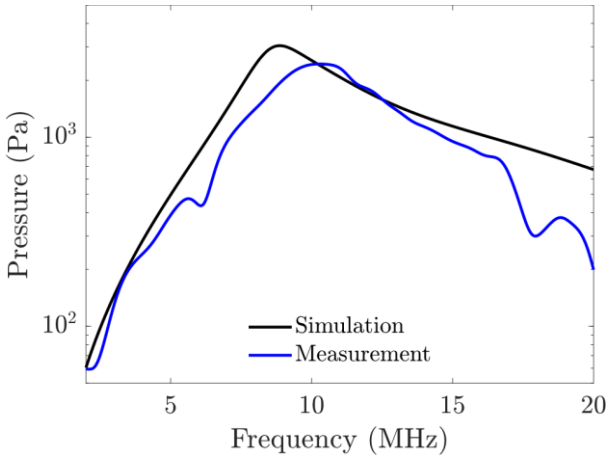

Figure 9: Output pressure at 10 cm as a function of frequency. Blue: experimental data. Black: analytical model.

The assessment of the performances of the PMUT as a sensor requires the development of a dedicated electronic that converts the charges induced by the incoming pressure on the membrane into an output voltage. The PMUT sensor delivers a current in the microampere range so that the electronics gain should be in the 10^4 – 10^5 range to reach tens to hundreds of millivolts. A transimpedance amplifier

(TIA) stage has therefore been designed with a 16 kΩ-gain at 10 MHz (Figure 10). The impedance matching of the TIA stage with the PMUT cell and the stability of the amplifier have also been carefully considered. A low-pass filter is added at the TIA output to remove out-of-band noise and match the 50Ω input impedance of the oscilloscope used for monitoring. Using such setup for reception and another calibrated PMUT for emission, the receive sensitivity at 10 MHz is measured at 9.6 V/MPa, which corresponds to a short-circuit sensitivity of 570 µA/MPa, i.e. 600 µA/MPa/mm².

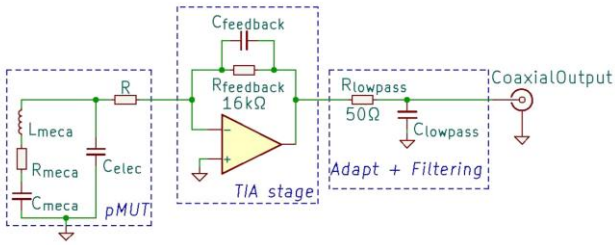

Figure 10: Schematic including the pMUT lumped element model and the electronics. The PMUT is modeled by a a Butterworth-Van Dyke lumped model fitted on experimental impedance measurements.

CONCLUSION

In this work, we achieved the design, the fabrication and the characterization of an AlN-based piezoelectric transducer. The key features of the device have been evaluated. There is a good agreement between measurements and simulation.

This works paves the way towards more specific devices that would benefit from the advantages of PMUT. There is still some room for improvement, regarding the piezoelectric material that may be changed for AlScN, what would increase the piezoelectric coefficient. The design of the single membrane and that of the cell could also be improved to obtain a larger bandwidth. Regarding the electronics, the signal-to-noise ratio is likely to be increased by adding a voltage amplifier stage after the transimpedance amplifier stage. PMUT could also benefit from MEMS interconnect technologies for miniaturization purpose or to build 2D arrays.

AKNOWLEDGEMENTS

This work has been funded by ECSEL Joint Undertaking project POSITION and by the Agence Nationale pour la Recherche (French National Agency for Research) through Carnot fundings. The authors also thank SOITEC for its support.

REFERENCES

[1] D. Horsley, « Ultrasonic Fingerprint Sensor Based on a PMUT Array Bonded to CMOS Circuitry », IEEE IUS 2016, 2016.

[2] R. J. Przybyla *et al.*, « In-Air Rangefinding With an AlN Piezoelectric Micromachined Ultrasound Transducer », *IEEE Sens. J.*, vol. 11, nº 11, p. 2690-2697, nov. 2011,

[3] E. Hardy *et al.*, « Spike-based Beamforming using PMUT Arrays for Ultra-Low Power Gesture Recognition », in *2022 International Electron Devices Meeting (IEDM)*, 2022, p. 24.4.1-24.4.4.

[4] Y. Qiu *et al.*, « Piezoelectric Micromachined Ultrasound Transducer (PMUT) Arrays for Integrated Sensing, Actuation and Imaging », *Sensors*, vol. 15, nº 4, p. 8020-8041, avr. 2015

[5] Y. Lu *et al.*, « Pulse-Echo Ultrasound Imaging Using an AlN Piezoelectric Micromachined Ultrasonic Transducer Array With Transmit Beam-Forming », *J. Microelectromechanical Syst.*, vol. 25, nº 1, p. 179-187, 2016

[6] B. E. Eovino *et al.*, « Concentric PMUT Arrays for Focused Ultrasound and High Intensity Applications », in *2019 IEEE 32nd International Conference on Micro Electro Mechanical Systems (MEMS)*, 2019, p. 771-774.

[7] Z. Liu *et al.*, « Characterization of Epitaxial-PZT/SI Piezoelectric Micromachined Ultrasonic Transducer (PMUT) and its Phased Array System », in *2019 20th International Conference on Solid-State Sensors, Actuators and Microsystems Eurosensors XXXIII*, juin 2019, p. 246-249

[8] « A European MEMS Ultrasound Benchmark » executed in the ECSEL Joint Undertaking project POSITION-2, https://www.s2e2.fr/wp-content/uploads/2022/03/CMUT-PMUT-Benchmark-Technical-Whitepaper.pdf

[9] Z. Liu *et al.*, « Fabrication and characterization of annular-shaped piezoelectric micromachined ultrasonic transducer mounted with Pb(Zr,Ti)O3-based monocrystalline thin film », *J. Micromechanics Microengineering*, vol. 31, nº 12, p. 125014, nov. 2021

[10] P. N. Thao *et al.*, « Development of mechanically-robust piezoelectric micromachined ultrasonic transducer based on island-shaped monocrystalline PZT thin film partially covered with polyimide », *J. Micromechanics Microengineering*, vol. 30, nº 12, p. 125015, nov. 2020

[11] Y. Huang *et al.*, « Implementing (K,Na)NbO3-based lead-free ferroelectric films to piezoelectric micromachined ultrasonic transducers », *Nano Energy*, vol. 103, p. 107761, 2022

[12] Y.-F. Wang *et al.*, « High-density PMUT array for 3-D ultrasonic imaging based on reverse-bonding structure », in *2011 IEEE 24th International Conference on Micro Electro Mechanical Systems*, Cancun, Mexico, janv. 2011, p. 1035-1038

[13] S. Pala *et al.*, « An Improved Lumped Element Model for Circular-Shape PMUTs », *IEEE Open J. Ultrason. Ferroelectr. Freq. Control*, vol. 2, p. 83-95, 2022

[14] J. Jung *et al.*, « Wafer-level experimental study of residual stress in AlN-based bimorph piezoelectric micromachined ultrasonic transducer », *Eng. Res. Express*, vol. 2, nº 4, p. 045013, oct. 2020

CONTACT

*B. Fain, bruno.fain@cea.fr